SolarPACES 2024, 30th International Conference on Concentrating Solar Power, Thermal, and Chemical Energy Systems

Analysis and Simulation of CSP and Hybridized System

https://doi.org/10.52825/solarpaces.v3i.2352

© Authors. This work is licensed under a Creative Commons Attribution 4.0 International License

Published: 18 Nov. 2025

# Modeling Thermochemical Energy Storage in a Solar Power Tower Plant: Dynamic Simulation

#### SolarPACES

Freddy Nieto<sup>1,\*</sup> , Alberto de la Calle<sup>2</sup>, and Rodrigo Escobar<sup>1,3</sup>

<sup>1</sup>Departamento de Ingeniería Mecánica y Metalúrgica, Pontificia Universidad Católica de Chile, Chile <sup>2</sup>Instituto de Catálisis y Petroleoquímica (ICP), CSIC, Spain

<sup>3</sup>Centro del Desierto de Atacama, Pontificia Universidad Católica de Chile, Chile

\*Correspondence: Freddy Nieto, fanieto@uc.cl

Abstract. This work presents a dynamic model of a novel Concentrated Solar Power plant that integrates Thermochemical Energy Storage with Calcium-Looping and a supercritical CO<sub>2</sub> Brayton power block. The aim is to provide a simulation tool to assess annual plant performance under realistic solar conditions. The model was developed using the Modelica language and simulated with OpenModelica. The configuration includes a heliostat field with a Solar Multiple of 1.8, 4 hours of TCES storage, and a 100 MW<sub>e</sub> sCO<sub>2</sub> Brayton cycle. The system effectively manages energy generation and storage through advanced control strategies, including defocusing to prevent overcharging and efficient handling of startup and shutdown phases. A parametric analysis was conducted to identify the optimal configuration, considering SM and storage hours variations. The results indicate that the highest plant efficiency and an LCOE below 110 USD/MWh are achieved with a solar multiple of approximately 2.6 and storage capacities exceeding 16 hours, aligning with ranges considered commercially viable for CSP technologies. However, the system exhibits higher radiation losses at the receiver due to the elevated reaction temperature. Despite this, the study demonstrates the energetic viability of the integrated CSP-TCES system. The findings highlight the potential of the proposed system, although ongoing efforts are aimed at further enhancing the model's accuracy.

**Keywords:** Performance Assessment, Calcium-Looping, Modelica, Supercritical CO<sub>2</sub>.

## 1. Introduction

Concentrated Solar Power (CSP) technology has advanced significantly over the past decade, particularly through the integration of Thermochemical Energy Storage (TCES) systems designed to enhance both dispatchability and efficiency. Among the promising approaches in this field is the Calcium-Looping (CaL) cycle, which leverages the reversible decomposition reaction of CaCO<sub>3</sub> into CaO and CO<sub>2</sub> to store and release thermal energy. This technology offers several advantages, including higher gravimetric and volumetric energy density that significantly reduce storage costs, the use of abundant and inexpensive natural materials such as limestone, the ability to operate at high temperature ranges (>900°C) and storage over extended periods, and a relatively low Levelized Cost of Energy (LCOE) when integrated with CSP systems. These factors make CaL particularly appealing for large-scale implementation [1],[2].

Since 2016, researchers have been exploring the feasibility and optimization of CaL systems within CSP plants, evaluating their performance in combination with various working fluids and cycle configurations. Chacartegui et al. [3] has focused on steady-state simulations of plant components and the direct integration of CaL with power cycles. While direct integration offers performance benefits, it also presents challenges, such as the need for more efficient power blocks and the requirement to pressurize the reactors [4],[5]. In recent years, research efforts have intensified to further optimize CaL systems. Ortiz et al. [6] investigated the integration of different power blocks with CaL, achieving a global integration efficiency at design conditions of 42% with a closed CO<sub>2</sub> Brayton cycle and conducting detailed thermal analyses across various operating temperatures. Carro et al. [7] reported a global plant efficiency of 36.23% using indirect integration of supercritical CO<sub>2</sub> (sCO<sub>2</sub>) with a recompression Brayton cycle.

Despite these advancements, several challenges persist, including sintering, the low reactivity of CaO, volume changes during reactions, and the need for dynamic simulations to test the system's real ability to adapt to the intermittency of the energy source. Nevertheless, current findings suggest that integrating CaL systems into CSP plants holds significant potential for reducing the LCOE and improving energy efficiency [5],[8], thereby covering the way for future commercialization. This study, therefore, focuses on the dynamic simulation of the integration of TCES-CaL within a SPT system.

# 2. System Description

Figure 1 presents a flow-sheet diagram of the proposed configuration, which integrates TCES-CaL in a SPT with a sCO<sub>2</sub> Brayton cycle. This system includes a heliostat field with a solar multiple of 1.8, a calciner reactor that serves as the receiver, 4 hours of TCES-CaL storage, and a carbonator connected to a 100 MWe sCO<sub>2</sub> Brayton power block with recompression. The TCES-CaL system operates based on the stoichiometric reaction equation (CaO + CO<sub>2</sub>  $\leftrightarrow$  CaCO<sub>3</sub> +Heat) [4]. The storage system is positioned in series between the receiver and the power block.

During solar operation, limestone from the mixed silo is fed into the receiver driven by the heat collected by the polar-layout heliostat field. In the calciner,  $CaCO_3$  undergoes an endothermic reaction, decomposing into solid CaO and gaseous  $CO_2$ . The solid CaO is stored in another silo, while the  $CO_2$  gas is stored in a pressure vessel at 72.3 bar and 31°C. The  $CO_2$  storage line is equipped with two air coolers, a compressor, an isothermal expander, and a heater to preheat the gas before carbonator. After storage, the exothermic reaction between CaO and  $CO_2$  occurs in the carbonator, which functions as a heat exchanger, generating the heat flow required by the power block. This thermal energy is then converted into electricity by the  $sCO_2$  Brayton cycle.

When solar energy is not available, the control system shuts down the calciner and operates the carbonator for discharge mode. Due to the high energy density of the system, a smaller storage size is required compared to conventional molten salt-based plants. Additionally, the lower thermal inertia of the sCO<sub>2</sub> Brayton cycle allows for faster start-ups and shut-downs. The plant control system monitors the levels in the two silos and the pressure vessel to manage the operation state of the calciner, carbonator, and heliostat field defocus mode.

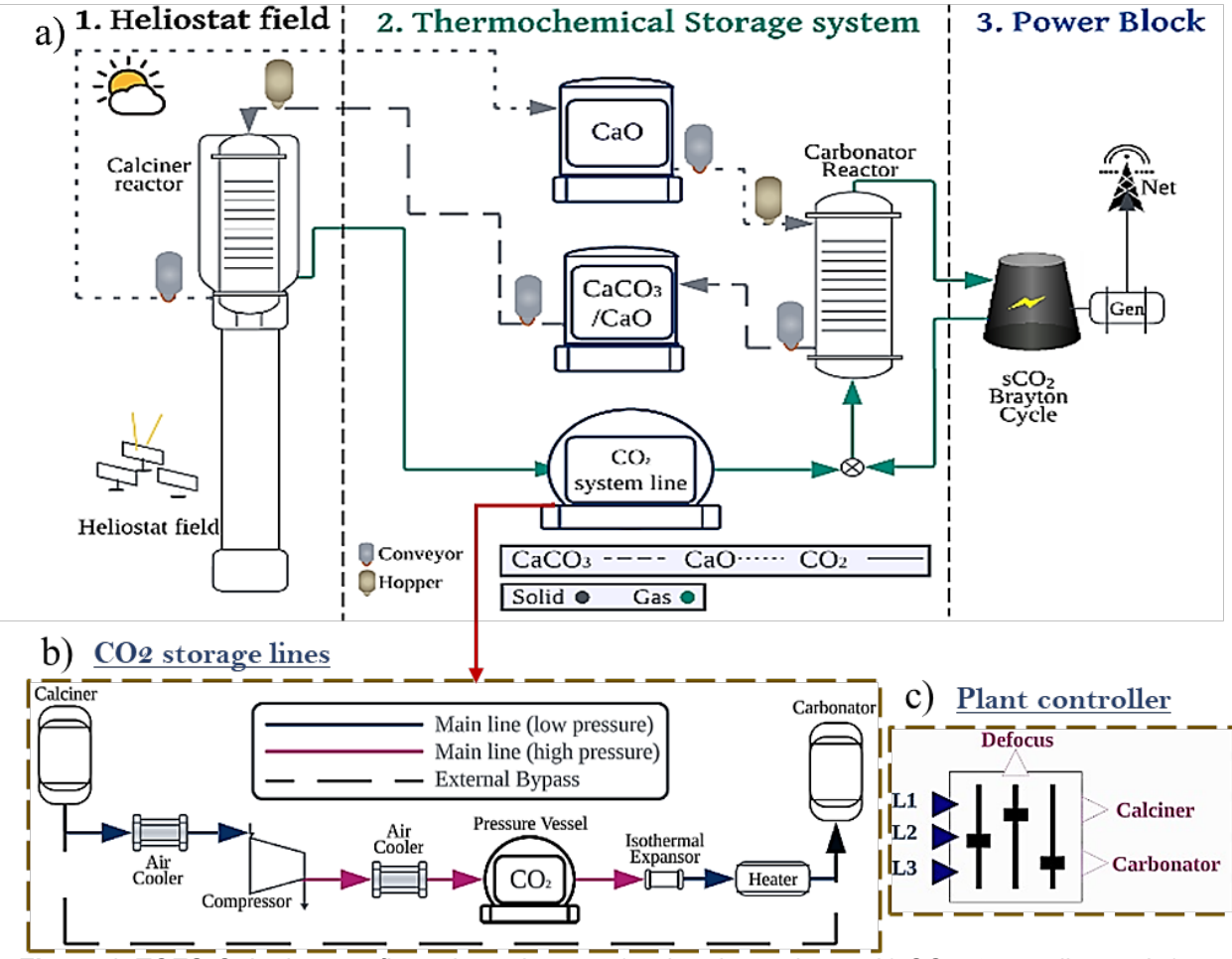


**Figure 1.** TCES-CaL plant configuration schemes a) solar plant scheme, b) CO₂ storage line and c) general control plant component.

## 2.1 General modelling approach

The model described in this section was implemented using the Modelica language [9]. Key physical and chemical phenomena were labeled and condensed into individual, reusable components, which were then interconnected to construct the final plant configuration. This modular approach offers a flexible tool for studying and optimizing various plant designs for maximum annual energy generation. The components adopted from the SolarTherm library include the data source, sun, heliostat field, silos, vessel, compressor, heaters, coolers, and the power cycle, all adapted to meet the specific requirements of the proposed system [10],[11]. In contrast, the reactor models (calciner and carbonator) were developed specifically for this work. A validation of the reactor models against reference data from the literature is presented in the following section.

The model was developed in OpenModelica 1.22.1 and is fully compatible with the Modelica Standard Library 4.0.0 (MSL). The Modelica Fluid connector facilitates data exchange between components, managing variables such as mass flow rate, pressure, specific enthalpy, and mass fraction. Meanwhile, the Modelica Thermal connector is used in the receiver to handle heat flow rate and temperature. Control signals are managed through single Boolean causal connectors. All components are internally balanced in terms of mass and energy, ensuring robust simulation and easier debugging [12]. Additionally, the techno-economic evaluation of the plant was conducted during the post-processing stage carried out using OMPython version 3.4.0, applying the LCOE methodology proposed by Meybodi et al. [13].

# 3. Subsystem Modelling

A short description of each model component is outlined below

**Media:** The medium models include equations for thermodynamic variables essential for mass and energy balances. To simulate the thermodynamic properties of CaCO<sub>3</sub> and CaO, polynomial expressions for specific heat capacity as a function of temperature are used [14]. For CO<sub>2</sub> thermodynamic properties, CoolProp [15] was utilized to generate tables containing enthalpy, entropy, and density as a function of pressure and temperature which are subsequently imported into OpenModelica.

**Data Source:** The data source model extracts weather data from a Typical Meteorological Year (TMY) file in the TMY3 format. This dataset contains hourly meteorological values representing typical conditions at a specific location over an extended period. A Python script converts the TMY file into a Modelica-readable table (MOTAB) format, making it readable in OpenModelica. Akima interpolation is then used to ensure a smooth and continuous derivative of the data during time simulation.

**Sun:** The sun model, adopted from the SolarTherm library, calculates the sun's position relative to the plant location and the Direct Normal Irradiance (DNI) at each time step. It employs equations developed by [16] to determine the solar vector, implemented as the PSA algorithm in the model.

Heliostat Field: This model calculates the total concentrated solar power of the heliostat field by considering the number of heliostats, heliostat area, availability, and total optical efficiency. The efficiency is provided as a table function calculated using SolarPILOT [17]. The efficiency accounts for factors such as cosine error, reflectivity, shading, blocking, attenuation, and spillage. The startup and shutdown of the plant are automatically controlled based on criteria like minimum starting power, operating power range, maximum wind speed, and minimum elevation angle.

**Reactors:** The stoichiometric balance in the reactors is based on the reaction equations for the calciner and carbonator. The models account for molar, mass, and energy balances, as well as residence time in the reactors. Conversion percentages of 100% and 40% are considered for the calciner and carbonator, respectively based on literature [1],[5]. The energy balance includes the required heat flow in the calciner associated with chemical reactions and radiation losses due to the high reaction temperature. Residence time in the reactors is modeled using an input time response function for each reactor [18],[19].

**Storage System:** The storage system comprises two silos for solids, one for CaO and the other for a mixture of CaCO $_3$  and CaO collected after the carbonation process, and a pressure vessel for the CO $_2$  gas. The material transportation system includes a lift for moving solids between silos and reactors. The silo model accounts for dynamic parameters such as mass, volume, area, and heat flow rates, including heat losses. For CO $_2$  storage, the gas exiting the calciner passes through an air cooler to reduce its temperature before entering the compressor at 40°C. It then passes through another air cooler to match the temperature of the pressure vessel. During discharge, the gas exits the pressure vessel, passes through an isothermal expander, and is preheated before entering the carbonator. If the system is in defocus mode, the gas bypasses the storage line and flows directly from the calciner to the carbonator, avoiding parasitic consumption in the CO $_2$  line.

**Power Cycle:** The power block calculates the gross and net electrical power generation. A regression model estimates the change in output variables relative to deviations from their design reference point. This regression model was developed using the off-design model by de la Calle et al. [20], based on Dyreby's work [21], which extrapolates experimental data on sCO<sub>2</sub> turbomachinery reported by Sandia National Laboratories. The gross electrical power is

calculated by summing the net electrical power and the parasitic loads of the plant, with startup thermal consumption also considered.

**Plant Control System:** This model controls the defocusing strategy and reactor operations based on the charge-discharge status, silo and pressure vessel levels, and solar resource availability. The mass flow rate is dynamically calculated within each model.

**Economic Model:** Formulas are based on literature and engineering estimates. The cost evaluation considers major components such as the heliostat field, tower, receiver, calciner, carbonator, TCES units (silos, vessels, compressors, and heat exchangers), applying scaling laws and correction factors. The LCOE, accounts for total capital cost, operating and maintenance costs, a 7% real discount rate, a 30-year plant lifetime, a 3-year construction period, and discounted annual net energy production [22-24].

# 4. System Modelling

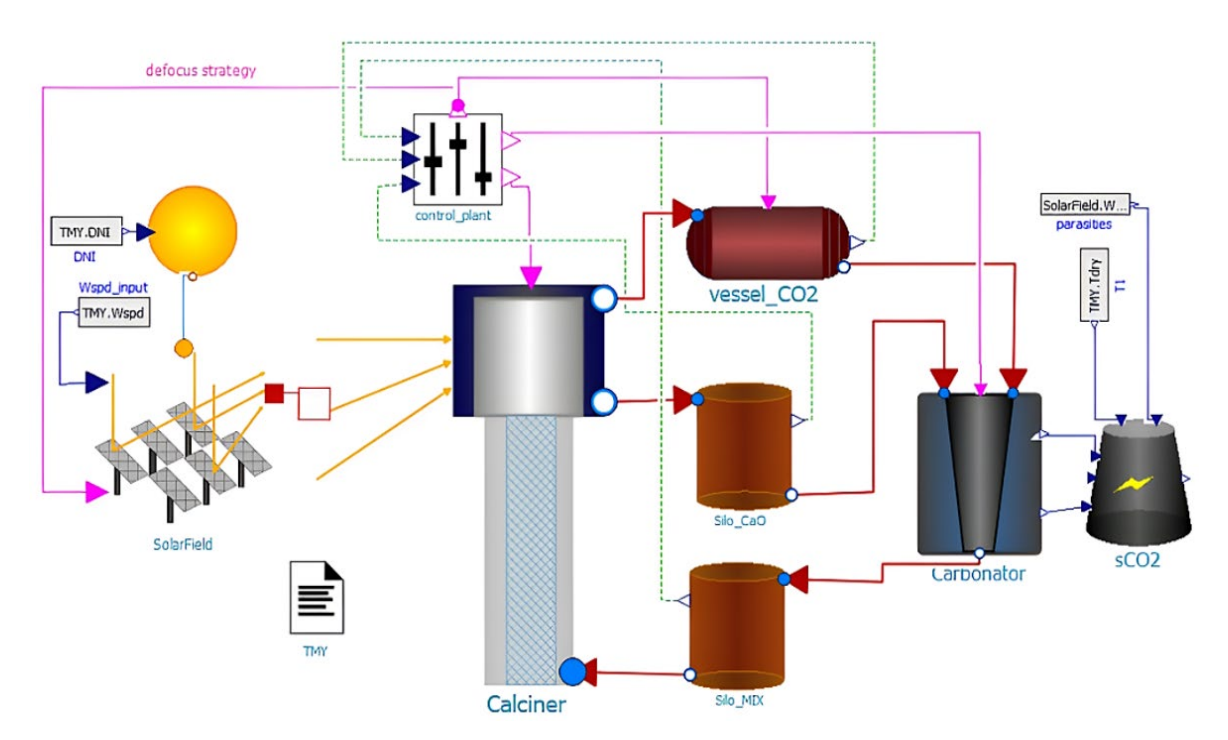


Figure 2. OpenModelica layout proposed plant configuration.

Figure 2 illustrates the final configuration of the proposed system model in the OpenModelica layout. The components are interconnected according to the scheme shown in Figure 1, where all elements of the CO<sub>2</sub> storage line are encapsulated within the vessel component. The model primarily uses DNI, ambient temperature, and wind speed as input variables, which are provided by the data source model.

#### 4.1 Reactors validation

The validation of the reactor models was carried out by comparing them against static models available in the literature, specifically those referenced in Table 1 and Table 2. The developed models were tested under the operating conditions proposed in each corresponding study, focusing mainly on the design heat input to the calciner ( $Q_{in}$ ), the conversion percentage (X), and, for the carbonator, the mass flow rate of CaO ( $m_{CaO,in}$ ) entering the reactor. Based on these operating conditions, the mass flow rates of the main components (CaO, CaCO<sub>3</sub>, and CO<sub>2</sub>) at the inlets and outlets were calculated. Table 1 and Table 2 present the representative mass flow rates for each component, comparing the results obtained from the OpenModelica

simulation with those reported in the literature. Additionally, the tables show the percentage difference (in parentheses) between the values, with deviations consistently below 3%.

**Table 1**. Validation of the Calciner Model: Comparison of Mass Flow Rates and Percentage Differences.

Ref.	Q <sub>in</sub> [MW]	Х	ṁ <sub>in</sub> [kg/s]		ṁ <sub>CO2,ou</sub>	t [kg/s]	mcaO,out [kg/s]		
			Paper	This work	Paper	This work	Paper	This work	
[1]	10e-3	0.1354	-	-	2e-3	2.03e-3 (1.47)	0.0174	0.0178 (2.25)	
[6]	100	0.15	216.56	215.31 (0.58)	22.81	22.68 (0.57)	193.75	192.63 (0.58)	
[25]	100	0.20	177.00	177.73 (0.41)	24.0	24.11 (0.46)	153.00	153.62 (0.40)	
[26]	100	0.15	215.80	215.31 (0.23)	22.77	22.68 (0.39)	193.02	192.63 (0.20)	
[5]	20.08	0.30	22.09	22.14 (0.23)	4.81	4.22 (12.26)	17.28	17.92 (3.57)	

**Table 2**. Validation of the Carbonator Model: Comparison of Mass Flow Rates and Percentage Differences.

	Q <sub>in</sub> [MW]	x	ṁ <sub>CaO,in</sub> [kg/s]	mc <sub>O2,in</sub> [kg/s]		ṁ <sub>CO2,out</sub>	[kg/s]	ṁ <sub>out</sub> [kg/s]	
Ref.				Paper	This work	Paper	This work	Pa- per	This work
[3]	100	0.50	31.04	196.9	199.14 (1.12)	184.7	186.95 (1.20)	212.4	214.67 (1.06)
[18]	100	0.15	64.58	133.72	131.02 (2.02)	126.25	123.42 (2.24)	72.19	72.18 (0.01)
[26]	100	0.50	64.30	133.9	130.21 (2.76)	-	-	-	-
[5]	20.08	0.30	17.28	20.41	20.32 (0.44)	16.34	16.25 (0.55)	21.36	21.35 (0.05)

## 5. Simulation

OpenModelica 1.22.1 was used for the Modelica implementations and simulations, with a differential/algebraic system solver (DASSL) as the numerical solver. The annual simulation was conducted using weather data from Daggett, USA. Figure 3 illustrates the performance of the TCES system over a five-day period starting from January 1st (3 sunny days and 2 partly cloudy days), configured with a solar multiple of 1.8 and 4 hours of storage capacity. In Figure 3a, the state of charge of the TCES system is shown, highlighting the charging, defocus and discharging periods. Notably, when the storage reaches its maximum capacity in sunny days, the system activates the defocusing mechanism (dashed lines) to prevent overcharging.

Figure 3b displays the heat input from the solar field, the projected heat flow, the heat generated during the carbonation process, and the net electrical work (W<sub>net</sub>). The W<sub>net</sub> curve (grey area) reveals the impact of parasitic power consumption by the compressor in the CO<sub>2</sub> storage line during the charging phase. It can be observed that on days with high solar variability, the heat flow is insufficient to store energy, resulting in limited energy generation. On sunny days, the system can generate power while simultaneously charging the TCES until reaching the defocus stage (green area) when storage is at its maximum capacity. This configuration demonstrates the system's ability to sustain energy generation during periods of lower solar input by effectively managing the charge and discharge cycles. The five-day period exemplifies the system's performance under varying solar resource conditions.

Figure 3c presents the annual energy distribution within the CSP plant, highlighting net energy and energy losses. Net energy, which represents the electricity generated by the plant, accounts for 17.72% of the total annual solar energy (2000 GWh). Parasitic losses, including energy consumed by auxiliary systems such as lifts, conveyor systems, and the compressor, constitute 3.89%. Thermal losses, representing energy lost as heat between the carbonator and the power block, amount to 21.29%. Receiver losses, primarily due to radiation losses from the high temperatures in the TCES system, account for 20.12%. Finally, defocus and

optical losses are the largest, at 6.81 and 30.16% respectively, associated with the defocus effect and optical efficiency calculated using SolarPILOT.

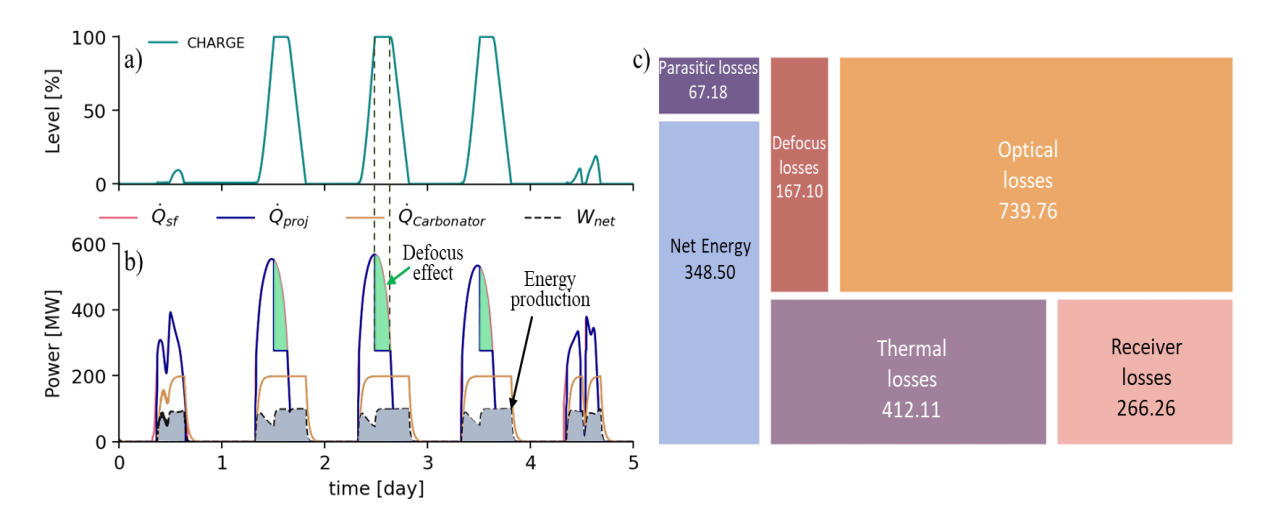


**Figure 3.** Simulation results a) charge level of the TCES, b) power and heat flows of the plant, c) LCOE vs storage hours and d) annual energy distribution of the plant in GWh.

Table 3 presents a comparison between a conventional reference case, a typical two-tank molten salt solar power plant with 100 MWe net capacity [27], and the proposed TCES plant with sCO<sub>2</sub> Brayton cycle, designed with the same parameters. Additionally, the storage hours for the proposed plant are varied to observe changes in its key performance indicators (KPIs) and to draw conclusions.

KPI	Reference	e TCES with sCO <sub>2</sub> Brayton cycle						
Solar multiple	1.8	1.8	1.8	1.8	1.8	1.8	1.8	-
Storage size	4	4	8	12	16	20	24	h
Annual energy	375.86	348.50	392.35	402.84	408.92	413.21	416.47	GWh
Capacity Factor	42.90	39.78	44.79	45.99	46.68	47.17	47.54	%
Plant efficiency	~18.00	17.42	19.61	20.13	20.44	20.65	20.82	%
LCOF	109 44	144 55	130 41	128 35	127 72	127 62	127 82	USD/MW/h

**Table 3**. KPIs of the reference and TCES-CaL plant configurations.

The reference plant was optimized for a solar multiple of 1.8 and 4 hours of storage, as a result, it generates more annual energy and has a 2% higher capacity factor compared to the proposed plant at the same design parameters. To identify the optimal performance point of the proposed plant, Table 3 shows that the improvement in KPIs (annual energy generation, capacity factor, plant efficiency and LCOE) becomes less pronounced once storage capacity exceeds 12 hours. Therefore, beyond 12 hours of storage, the additional benefits in terms of KPIs tend to diminish. In the LCOE comparison, the proposed plant exhibits higher values than the reference plant, as the latter is already optimized for its specific SM and storage hours. In contrast, the proposed configuration requires a parametric analysis to identify its optimal operating range. This analysis is presented in Figure 4.

Figure 4 presents a parametric analysis of the proposed plant, exploring variations in the SM from 1.4 to 3.6 in increments of 0.4, alongside a range of storage capacities from 1 to 24 hours. The objective of this analysis is to identify the design parameters that yield the best KPIs for the proposed plant configuration. In Figure 4a, the dotted curves indicate configurations with a 55% and 65% capacity factor, which are directly associated with the highest annual energy generation. Conversely, Figure 4b illustrates the overall plant efficiency, where the best efficiency results are located within the boundary areas marked by dashed lines. These values

align with the commercially viable range for CSP plants. The intersection of the areas representing the highest energy generation and plant efficiency indicates that the optimal configurations are found with solar multiples between 2.4 and 2.7, and storage capacities exceeding 12 hours.

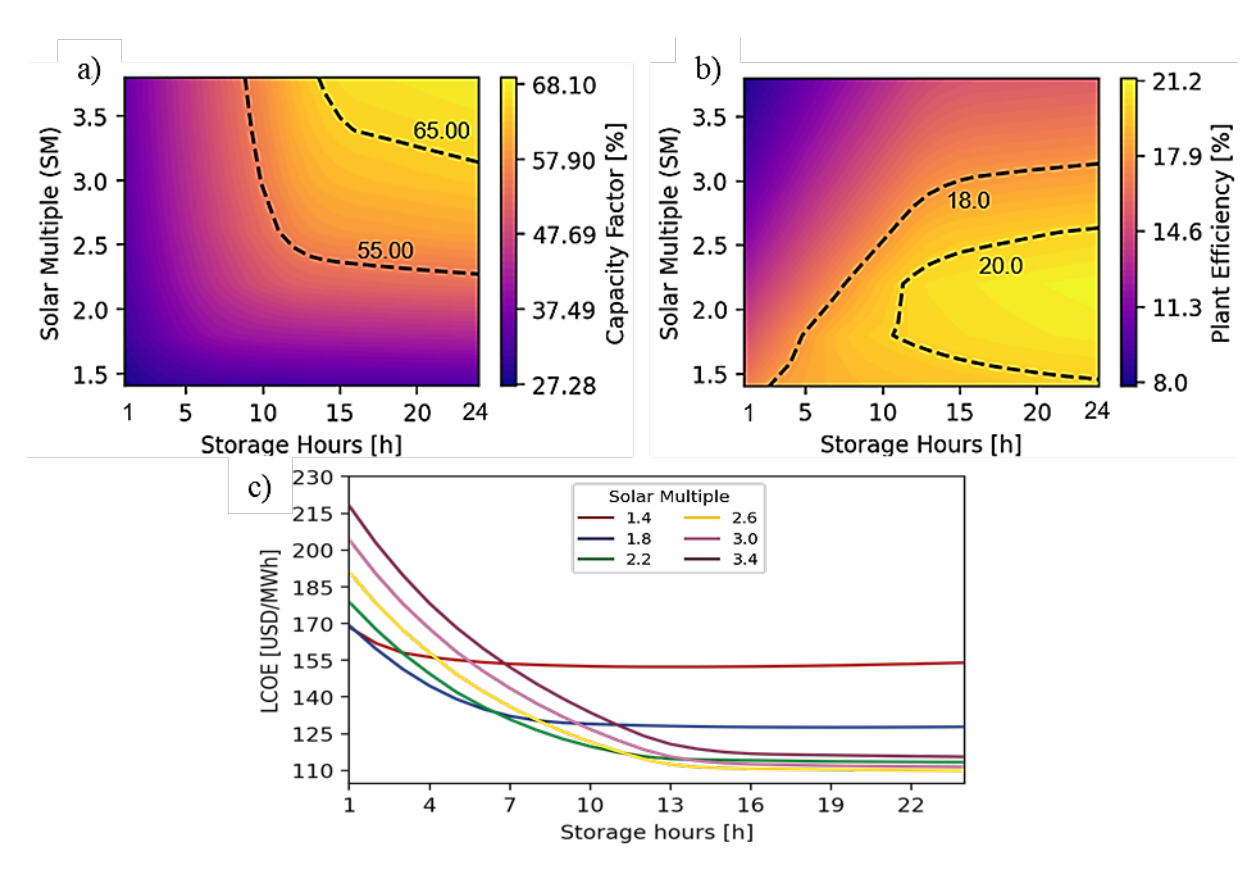


**Figure 4.** Parametric analysis of the storage characterization based on SM and STO a) Capacity factor, b) plant efficiency and c) LCOE of the proposed plant.

Figure 4c presents the parametric analysis of the LCOE for the proposed plant. As expected, the LCOE decreases with increasing storage duration across all curves. Notably, the curve corresponding to SM = 2.6 achieves the lowest LCOE values, reaching levels below 110 USD/MWh for storage durations exceeding 16 hours.

## 6. Conclusions

In this work, a new dynamic model of an innovative solar power plant integrating TCES-CaL and a  $sCO_2$  Brayton cycle is presented. The promising results suggest that the system could be energetically viable, although higher radiation heat losses at the receiver were noted due to the elevated reaction temperatures. The model was compared with a typical two-tank molten salt solar power plant with a net capacity of 100 MWe, and the reactor components were validated against static models reported in the literature. Significant advantages were observed in terms of capacity factor and plant efficiency, mainly attributed to the optimization of the system for the selected solar multiple and storage hours. As shown in Table 3, at higher storage capacities, the proposed plant outperforms the reference configuration by approximately 4.5% in capacity factor and 2.8% in plant efficiency. Furthermore, Figure 4 shows that the most suitable operating conditions for the proposed system occur for solar multiples between 2.4 and 2.7 with storage capacities above 12 hours, with the lowest LCOE values obtained for SM = 2.6 and storage durations greater than 16 hours.

Future work will focus on conducting a more detailed optimization study, exploring alternative CO<sub>2</sub> storage configurations to reduce parasitic energy consumption, and proposing new system layouts. While the current results are promising, ongoing improvements aim to further enhance the model's accuracy and predictive capabilities.

## **Author contributions**

Freddy Nieto: Conceptualization, Software, Formal analysis, Methodology, Writing – original draft, Writing – review & editing. Alberto de la Calle: Supervision, Writing – review & editing. Rodrigo Escobar: Supervision, Funding acquisition, Writing – review & editing.

# Competing interests

The authors declare that they have no competing interests.

# Acknowledgement

F. Nieto would like to acknowledgment to Vicerrectoría de Investigación de la Pontificia Universidad Católica de Chile for their sponsorship towards the development of this research. Additionally, to the "Grupo Solar UC" for their scientific support.

## References

- [1] M. Bailera, S. Pascual, P. Lisbona, and L. M. Romeo, "Modelling calcium looping at industrial scale for energy storage in concentrating solar power plants," Energy, vol. 225, p. 120306, Jun. 2021, doi: <a href="https://doi.org/10.1016/J.ENERGY.2021.120306">10.1016/J.ENERGY.2021.120306</a>.
- [2] B. Moghtaderi and A. Seyfaee, "A multi-scale experimental study on calcium-looping for thermochemical energy storage using the CO2 captured from power generation systems," J Energy Storage, vol. 86, p. 111400, May 2024, doi: 10.1016/J.EST.2024.111400.
- [3] R. Chacartegui, A. Alovisio, C. Ortiz, J. M. Valverde, V. Verda, and J. A. Becerra, "Thermochemical energy storage of concentrated solar power by integration of the calcium looping process and a CO2 power cycle," Appl Energy, vol. 173, pp. 589–605, Jul. 2016, doi: 10.1016/j.apenergy.2016.04.053.
- [4] U. Tesio, E. Guelpa, and V. Verda, "Integration of thermochemical energy storage in concentrated solar power. Part 1: Energy and economic analysis/optimization," Energy Conversion and Management: X, vol. 6, p. 100039, Apr. 2020, doi: 10.1016/J.ECMX.2020.100039.
- [5] Q. Xu, Iwei Wang, Z. Li, and L. Shi, "A calcium looping system powered by renewable electricity for long-term thermochemical energy storage, residential heat supply and carbon capture," Energy Convers Manag, vol. 276, p. 116592, Jan. 2023, doi: 10.1016/J.ENCONMAN.2022.116592.
- [6] C. Ortiz, R. Chacartegui, J. M. Valverde, A. Alovisio, and J. A. Becerra, "Power cycles integration in concentrated solar power plants with energy storage based on calcium looping," Energy Convers Manag, vol. 149, pp. 815–829, Oct. 2017, doi: <a href="https://doi.org/10.1016/j.enconman.2017.03.029">10.1016/j.enconman.2017.03.029</a>.
- [7] Carro, R. Chacartegui, C. Ortiz, and J. A. Becerra, "Indirect power cycles integration in concentrated solar power plants with thermochemical energy storage based on calcium hydroxide technology," J Clean Prod, vol. 421, p. 138417, Oct. 2023, doi: 10.1016/J.JCLEPRO.2023.138417.
- [8] J. Zhao et al., "Particle-based high-temperature thermochemical energy storage reactors," Prog Energy Combust Sci, vol. 102, p. 101143, May 2024, doi: 10.1016/J.PECS.2024.101143.

- [9] Modelica Association, "Modelica® Language Specification version 3.6." Accessed: Jul. 31, 2024. [Online]. Available: <a href="https://specification.modelica.org/maint/3.6/MLS.html">https://specification.modelica.org/maint/3.6/MLS.html</a>
- [10] de la Calle, J. Hinkley, P. Scott, and J. Pye, "SolarTherm: A New Modelica Library and Simulation Platform for Concentrating Solar Thermal Power Systems," SNE Simulation Notes Europe, vol. 28, no. 3, pp. 101–103, Sep. 2018, doi: 10.11128/sne.28.sn.10427.
- [11] P. Scott, A. D. L. C. Alonso, J. T. Hinkley, and J. Pye, "SolarTherm: A flexible Modelica-based simulator for CSP systems," AIP Conf Proc, vol. 1850, Jun. 2017, doi: 10.1063/1.4984560.
- [12] H. Olsson, M. Otter, S. E. Mattsson, and H. Elmqvist, "Balanced Models in Modelica 3.0 for Increased Model Quality," 2008.
- [13] Meybodi, M. A., & Beath, A. C. (2016). Impact of cost uncertainties and solar data variations on the economics of central receiver solar power plants: An Australian case study. Renewable Energy, 93, 510–524. <a href="https://doi.org/10.1016/J.RENENE.2016.03.016">https://doi.org/10.1016/J.RENENE.2016.03.016</a>.
- [14] NIST, "Standard Reference Data | NIST." Accessed: Nov. 12, 2023. [Online]. Available: https://www.nist.gov/srd
- [15] H. Bell, J. Wronski, S. Quoilin, and V. Lemort, "Pure and pseudo-pure fluid thermophysical property evaluation and the open-source thermophysical property library coolprop," Ind Eng Chem Res, vol. 53, no. 6, pp. 2498–2508, Feb. 2014, doi: 10.1021/IE4033999/SUPPL\_FILE/IE4033999\_SI\_002.ZIP.
- [16] M. Blanco-Muriel, D. C. Alarcón-Padilla, T. López-Moratalla, and M. Lara-Coira, "Computing the solar vector," Solar Energy, vol. 70, no. 5, pp. 431–441, Jan. 2001, doi: 10.1016/S0038-092X(00)00156-0.
- [17] M. J. Wagner and T. Wendelin, "SolarPILOT: A power tower solar field layout and characterization tool," Solar Energy, vol. 171, pp. 185–196, Sep. 2018, doi: 10.1016/J.SOLENER.2018.06.063.
- [18] Scaltsoyiannes and A. Lemonidou, "CaCO3 decomposition for calcium-looping applications: Kinetic modeling in a fixed-bed reactor," Chemical Engineering Science: X, vol. 8, p. 100071, Nov. 2020, doi: <a href="https://doi.org/10.1016/J.CESX.2020.100071">10.1016/J.CESX.2020.100071</a>.
- [19] Ortiz, J. M. Valverde, R. Chacartegui, and L. A. Perez-Maqueda, "Carbonation of Limestone Derived CaO for Thermochemical Energy Storage: From Kinetics to Process Integration in Concentrating Solar Plants," ACS Sustain Chem Eng, vol. 6, no. 5, pp. 6404–6417, May 2018, doi: 10.1021/ACSSUSCHEMENG.8B00199.
- [20] de la Calle, A. Bayon, and Y. C. Soo Too, "Impact of ambient temperature on supercritical CO2 recompression Brayton cycle in arid locations: Finding the optimal design conditions," Energy, vol. 153, pp. 1016–1027, Jun. 2018, doi: 10.1016/J.EN-ERGY.2018.04.019.
- [21] Dyreby, "Modeling the Supercritical Carbon Dioxide Brayton Cycle with Recompression," 2014.
- [22] Turchi, Craig S., Matthew Boyd, Devon Kesseli, Parthiv Kurup, Mark Mehos, Ty Neises, Prashant, Sharan, Michael Wagner, & Timothy Wendelin. (2019). CSP Systems Analysis Final Project Report. In NREL. <a href="https://www.nrel.gov/docs/fy19osti/72856.pdf">https://www.nrel.gov/docs/fy19osti/72856.pdf</a>
- [23] Bayon, A., Bader, R., Jafarian, M., Fedunik-Hofman, L., Sun, Y., Hinkley, J., Miller, S., & Lipiński, W. (2018). Techno-economic assessment of solid–gas thermochemical energy storage systems for solar thermal power applications. *Energy*, 149, 473–484. https://doi.org/10.1016/J.ENERGY.2017.11.084.
- [24] Starke, A. R., Cardemil, J. M., Bonini, V. R. B., Escobar, R., Castro-Quijada, M., & Videla, Á. (2024). Assessing the performance of novel molten salt mixtures on CSP applications. *Applied Energy*, 359, 122689. <a href="https://doi.org/10.1016/J.APEN-ERGY.2024.122689">https://doi.org/10.1016/J.APEN-ERGY.2024.122689</a>.
- [25] Alovisio, A., Chacartegui, R., Ortiz, C., Valverde, J. M., & Verda, V. (2017). Optimizing the CSP-Calcium Looping integration for Thermochemical Energy Storage. *Energy Conversion and Management*, 136, 85–98. <a href="https://doi.org/10.1016/j.encon-man.2016.12.093">https://doi.org/10.1016/j.encon-man.2016.12.093</a>.

- [26] Bravo, R., Ortiz, C., Chacartegui, R., & Friedrich, D. (2021). Multi-objective optimisation and guidelines for the design of dispatchable hybrid solar power plants with thermochemical energy storage. *Applied Energy*, 282, 116257. <a href="https://doi.org/10.1016/j.apenergy.2020.116257">https://doi.org/10.1016/j.apenergy.2020.116257</a>.
- [27] de la Calle, A. Bayon, and J. Pye, "Techno-economic assessment of a high-efficiency, low-cost solar-thermal power system with sodium receiver, phase-change material storage, and supercritical CO2 recompression Brayton cycle," Solar Energy, vol. 199, pp. 885–900, Mar. 2020, doi: 10.1016/J.SOLENER.2020.01.004.